

Antiferromagnetic iron-based magnetoelectric compoundsS. W. Lovesey *ISIS Facility, STFC, Didcot, Oxfordshire OX11 0QX, United Kingdom;
Diamond Light Source, Harwell Science and Innovation Campus, Didcot, Oxfordshire OX11 0DE, United Kingdom;
and Department of Physics, Oxford University, Oxford OX1 3PU, United Kingdom*

(Received 3 December 2022; accepted 14 April 2023; published 28 April 2023)

The Landau free energy of a compound that benefits from a linear coupling of an electric field and a magnetic field includes a product of the two fields, one polar and time even and one axial and time odd. Evidently, the coefficient of the product of fields is unchanged by a simultaneous change in the directions of space and time, a symmetry operation labeled anti-inversion. Invariance with respect to anti-inversion is the defining symmetry of the linear magnetoelectric (ME) effect included in 58 of 122 magnetic crystal classes, 19 of which prohibit higher-order (nonlinear) contributions to the free energy. In ME compounds, expectation values of some atomic magnetic tensors are invariant with respect to anti-inversion. An invariance shared by the Dirac monopole (an element of charge allowed in Maxwell's equations that has not been observed) and a Zel'dovich anapole, is also known as a Dirac dipole. From the science of materials perspective, it has been established that Dirac multipoles contribute to the diffraction of x rays and neutrons. We identify Dirac monopoles in bulk magnetic properties of iron tellurate (Fe_2TeO_6) and a spin ladder ($\text{SrFe}_2\text{S}_2\text{O}$). They are visible in the diffraction of light using an iron electric dipole–magnetic dipole absorption event. Both cited compounds present a simple antiferromagnetic configuration of axial dipoles, and their different magnetic crystal classes allow a linear ME effect. However, the Kerr effect is symmetry allowed in the spin ladder and forbidden in iron tellurate. Anapoles are forbidden in iron tellurate and allowed in the spin ladder compound, a difference evident in diffraction patterns fully informed by symmetry. More generally, we identify a raft of Dirac multipoles, and axial multipoles beyond dipoles, visible in future experiments using standard techniques with beams of neutrons or x rays tuned in energy to an iron atomic resonance. ME invariance imposes a phase relationship between nuclear (charge) and magnetic contributions to neutron (x-ray) diffraction amplitudes. In consequence, intensities of Bragg spots in an x-ray pattern do not change when helicity in the primary beam is reversed. A like effect occurs in the magnetic diffraction of polarized neutrons.

DOI: [10.1103/PhysRevB.107.144432](https://doi.org/10.1103/PhysRevB.107.144432)**I. INTRODUCTION**

The induction of magnetization by an electric field, and the inverse magnetoelectric (ME) effect, namely, induction of electric polarization by a magnetic field, have been studied for a long time. In 1959, Dzyaloshinskii predicted that a linear coupling of the two fields could occur in antiferromagnetic chromium sesquioxide (Cr_2O_3) [1]. A year later, the coupling coefficient was experimentally observed to be nonzero in an unorientated crystal below the Néel temperature [2]. Further early work on the ME effect in Cr_2O_3 and other antiferromagnetic crystals, such as Gd_2CuO_4 , Sm_2CuO_4 , KNiPO_4 , LiCoPO_4 , and BiFeO_3 , is gathered in Refs. [3,4]. The ME effect is allowed when the magnetic crystal class contains the product of spatial and time inversions, or anti-inversion ($\bar{1}'$); i.e., the two discrete symmetries of space and time do not occur independently. Specifically, the linear ME coupling

coefficient in the Landau free energy is unchanged by a simultaneous change in sign of space and time coordinates. Of 58 classes that allow the linear ME effect, there are 19 that do not allow nonlinear effects. Examples of the 19 linear types include trigonal Cr_2O_3 (magnetic crystal class $\bar{3}'m'$) and tetragonal gadolinium tetraboride GdB_4 ($4/m' m' m'$) [5,6].

Anti-inversion in the crystal class prohibits axial magnetism, which is parity even (axial) and time odd (magnetic). Magnetic monopoles are allowed, however. While there is a strong symmetry between electric and magnetic fields in Maxwell's equations, a magnetic charge analogous to electric charge is peculiarly absent. If the equations are symmetrized by the introduction of magnetic charge, this charge must be such that it is reversed by each of the discrete symmetries of parity and time [7]. At an atomic level of detail, a monopole $\langle \mathbf{S} \cdot \mathbf{R} \rangle$ represents magnetic charge, where \mathbf{S} and \mathbf{R} are spin and orbital electronic degrees of freedom, respectively, and angular brackets denote a time average (expectation value). Such a charge contributes to the diffraction of x rays utilizing an electric dipole–magnetic dipole event [8–10]. Notably, a magnetic charge and Dirac's monopole have identical discrete symmetries [7,11]. An anapole is the next member along in a family of electronic Dirac multipoles and it is equivalent to a

Published by the American Physical Society under the terms of the Creative Commons Attribution 4.0 International license. Further distribution of this work must maintain attribution to the author(s) and the published article's title, journal citation, and DOI.

TABLE I. Properties of antiferromagnetic iron-based ME compounds. The propagation vector $= (0, 0, 0)$, space groups are centrosymmetric, the piezomagnetic effect is forbidden, and α_{jj} are diagonal components of the third-order ME coupling tensor. Magnetic ions occupy sites $4(e)$. Saturation magnetic moments are in units of the Bohr magneton μ_B . Our investigation of the orthorhombic compound applies also to $\text{SrFe}_2\text{Se}_2\text{O}$ with a different Néel temperature T_N and cell edges [28].

Fe_2TeO_6 [23,24]	$\text{SrFe}_2\text{S}_2\text{O}$ [28]
Tetragonal	Orthorhombic
$P4_2/m'n'm'$ (No. 136.503)	$Pm'm'n'$ (No. 59.411)
$4/m'm'm'$	$m'm'm'$
$\text{Fe}^{3+}(3d^5)$	$\text{Fe}^{2+}(3d^6)$
$\alpha_{11}, \alpha_{11}, \alpha_{33}$	$\alpha_{11}, \alpha_{22}, \alpha_{33}$
$T_N \approx 209$ K	$T_N \approx 216$ K
$\mu \approx 4.2 \mu_B$	$\mu \approx 3.3 \mu_B$
Monopole	Monopole
No anapole	Anapole
No Kerr effect	Kerr effect [56]

dipole $\langle (\mathbf{S} \times \mathbf{R}) \rangle$ and a like orbital entity [12–14]. The Dirac monopole and the anapole represent the scalar (rank $K = 0$) and dipole ($K = 1$) in a decomposition of the third-rank ME tensor coupling coefficient. Anapoles contribute to the Bragg diffraction of x rays and neutrons, along with higher-order multipoles, e.g., a quadrupole ($K = 2$) in the decomposition of the ME coefficient [15–17]. Compton scattering of x rays is another technique with potential to observe them [18,19]. Advanced simulations of electronic structure are established methods by which to derive estimates of Dirac multipoles [20–22].

Looking to the future, we calculate Bragg diffraction patterns for two antiferromagnetic iron-based magnetoelectric materials specified in Table I. The configuration of axial magnetic dipoles in iron tellurate (Fe_2TeO_6), depicted in Fig. 1, was established in 1968 [23], and its magnetoelectric properties are firmly established [24–27]. This is not so for the

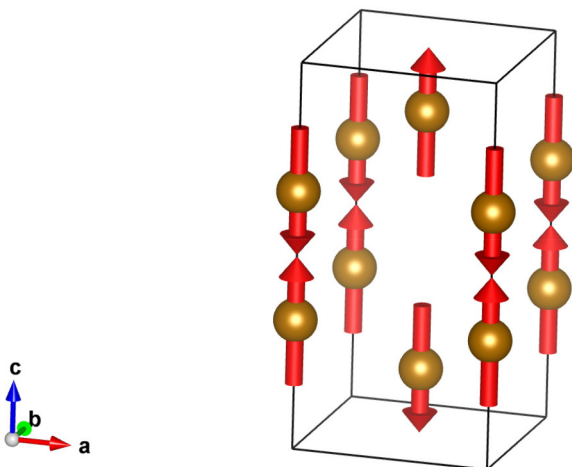


FIG. 1. Configuration of ferric axial magnetic dipoles in the inverted trirutile Fe_2TeO_6 [23]. Reproduced from MAGNDATA [29].

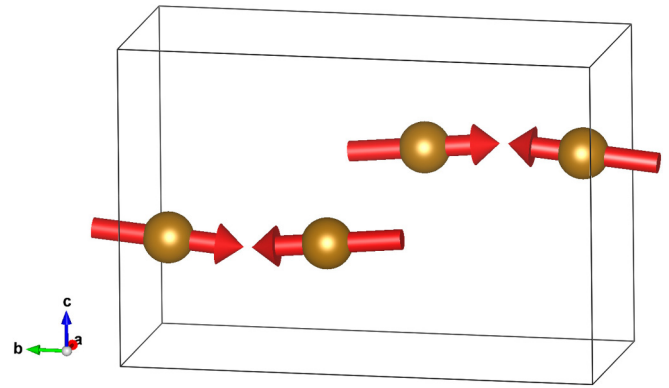


FIG. 2. Configuration of ferrous axial magnetic dipoles in the orthorhombic spin ladder compound $\text{SrFe}_2\text{S}_2\text{O}$ [28]. Reproduced from MAGNDATA [29].

spin ladder compound $\text{SrFe}_2\text{S}_2\text{O}$, to the best of our knowledge [28]. Axial magnetic dipoles for the spin ladder are depicted in Fig. 2, and the same configuration has been established for $\text{SrFe}_2\text{Se}_2\text{O}$ [28]. All mentioned magnetic configurations have a propagation vector $= (0, 0, 0)$, and magnetic space groups are centrosymmetric.

Anti-inversion among the elements of symmetry in a magnetic crystal class is a profound influence on diffraction amplitudes. For Bragg diffraction of x rays enhanced by an atomic resonance, charge and magnetic contributions to scattering amplitudes are in phase [30]. Thus, there is no interference between charge and magnetic contributions to Bragg diffraction patterns gathered from a ME compound. Moreover, coupling to helicity in primary x rays is forbidden, with no difference in the intensity of a Bragg spot observed with opposite-handed x rays. In contrast, anti-inversion invariance imposes a 90° phase shift between nuclear and magnetic contributions in neutron scattering, and they are in quadrature in the intensity of a Bragg spot [5,31,32]. A corollary is that the classical polarized neutron diffraction technique, using a departure from unity of the ratio of intensities for primary neutron beams of opposite polarization, is not available for ME compounds [31,33–35]. In their measurement of the magnetization distribution in Cr_2O_3 , Brown *et al.* exploited spherical neutron polarimetry [5].

Valence states accessed by photoejected electrons interact with neighboring ions when x rays excite a core resonance. Thus, electronic multipoles in the ground state observed in diffraction are rotationally anisotropic with a symmetry corresponding to the site symmetry of the resonant ion. The distribution in a crystal of spherically symmetric atomic charge defines a space group. In general, strong Bragg spots are absent in diffraction for specific conditions on Miller indices, and absence conditions are listed in the Appendix for the two compounds of interest. Absence conditions can be violated by relatively weak Bragg spots arising from nonspherical atomic charge, which is usually called Templeton-Templeton scattering [36–38]. Space group forbidden Bragg spots are particularly revealing with regard to fine features of the electronic structure. Tuning the energy of x rays to an atomic resonance has two obvious benefits. In the first place, there is a welcome enhancement of Bragg spot

intensities and, secondly, spots are element specific. There are four scattering amplitudes labeled by photon polarization, two with unrotated and two with rotated states of polarization [13,38]. Strong Thomson scattering, by spherically symmetric atomic charge, that overwhelms weak signals is absent in rotated channels of polarization. It is allowed in unrotated channels of polarization using a parity-even absorption, but is absent in a parity-odd absorption, e.g., electric dipole–electric dipole (E1-E1) and electric dipole–electric quadrupole (E1-E2) events. Diffraction amplitudes for E1-E1, E2-E2, and E1-E2 events presented here include rotation of the crystal about the reflection vector (azimuthal-angle scan) and they are specific to position multiplicity, Wyckoff letter, and symmetry [38]. The range of values of the rank K is fixed by the triangle rule, and $K = 0-2$, $K = 1-3$, and $K = 0-4$ for E1-E1, E1-E2, and E2-E2 events, respectively. Angular rotation symmetry in a crystal can be mirrored in a periodicity of an azimuthal-angle scan, and the valuable property of the diffraction technique depends on the direction of the chosen reflection vector relative to crystal axes.

Magnetic multipoles in x-ray diffraction using E1-E1 or E2-E2 absorption events have an odd rank, i.e., $K = 1$ or 3 [13,38], whereas a parity-odd E1-E2 event presents Dirac multipoles with $K = 1, 2$, and 3 . Magnetic contributions to neutron diffraction patterns are often identified in differences between patterns taken at different temperatures, above and below the onset of long-range magnetic order. Greater sensitivity is afforded by exploiting polarization analysis. A spin-flip signal has been used to good effect in measuring weak magnetic signals from long-range order in the pseudogap phase of high-temperature superconducting cuprates [39–43].

Bulk magnetic properties of iron tellurate are made exclusively of Dirac multipoles, including monopoles. Although anapoles are forbidden, Dirac multipoles alone are responsible for a whole class of Bragg spots for which we give scattering amplitudes fully informed by symmetry. Axial quadrupoles produce weak (space group forbidden) reflections. They account for a correlation between anapole and orbital degrees of freedom in the magnetic neutron scattering amplitude. An axial secondary order parameter in the spin ladder compound contributes weak Bragg spots. Axial dipoles and anapoles are orthogonal, with anapoles confined to the a axis in Fig. 2. However, anapoles do not contribute to bulk properties of $\text{SrFe}_2\text{S}_2\text{O}$. A Kerr effect is allowed, unlike iron tellurate.

II. IRON TELLURATE

The rutile-type structure (space group $P4_2/mnm$) contains chains of edge-sharing octahedra along the crystal c axis joined through corners in the $a-b$ plane. Trirutile materials (AB_2X_6 composition) use a superstructure with a tripling of the rutile unit along the c axis [44]. Antiferromagnetic chains parallel with the $[1, 1, 0]$ axis, distinguished by the closest metal-metal separation in a trirutile, are a characteristic of the magnetic states [45]. The compound of interest, Fe_2TeO_6 , is referred to as an “inverted” trirutile, because the A and B cations are interchanged with respect to the nominal trirutile [46]. It displays a linear magnetoelectric effect (ME), as does Cr_2WO_6 [47,48]. The mentioned trirutile oxides possess

different long-range magnetic structures and magnetic crystal classes, however, with moments parallel (Fe, $4/m'm'm'$) and perpendicular (Cr, $m'mm$) to the c axis [23].

Absence conditions on Miller indices (h, k, l) for Bragg diffraction by $P4_2/mnm$ are listed in the Appendix. The configuration of axial magnetic dipoles depicted in Fig. 1 belongs to the tetragonal centrosymmetric space group $P4_2/m'n'm'$ (No. 136.503 BNS [49]), and ME crystal class $4/m'm'm'$. Ferric ions (Fe^{3+} , $3d^5$) are in noncentrosymmetric Wyckoff sites $4(e)$, with site symmetry $2.m'm'$ comprising two operations 2_z (dyad axis of rotation symmetry along the c axis in Fig. 1) and m'_{xy} (mirror and time-reversal invariances along a diagonal in the $a-b$ plane). Cell lengths $a \approx 4.601 \text{ \AA}$ and $c \approx 9.087 \text{ \AA}$, and $T_N \approx 209 \text{ K}$ [23]. There are two independent parameters in the ME coupling (susceptibility) tensor [24]. A piezomagnetic effect is forbidden by anti-inversion in the crystal class.

Properties of antiferromagnetic Fe_2TeO_6 contrast with those of MnF_2 [50], CoF_2 , and FeF_2 that also have the rutile structure $P4_2/mnm$. Magnetic properties of the cited fluorides belong to the centrosymmetric crystal class $4'/mmm'$. The absence of anti-inversion in the crystal class means that the ME effect is nonlinear, a piezomagnetic effect is allowed, and the classical polarized neutron diffraction technique is available [5,31,32].

A. X-ray diffraction

A universal structure factor of rank K ,

$$\Psi_Q^K = [\exp(i\boldsymbol{\kappa} \cdot \mathbf{d})] \cdot \langle O_Q^K \rangle_{\mathbf{d}}, \quad (1)$$

determines diffraction amplitudes. An electronic multipole $\langle O_Q^K \rangle$ possesses $(2K + 1)$ projections in the interval $-K \leq Q \leq K$, and the complex conjugate obeys $(-1)^Q \langle O_{-Q}^K \rangle = \langle O_Q^K \rangle^*$. Multipoles for x-ray and neutron scattering abide by the same discrete symmetry requirements but they are different in detail. The structure factor Ψ_Q^K is informed of all elements of symmetry in the magnetic space group. In Eq. (1), $\boldsymbol{\kappa}$ is the reflection vector defined by integer Miller indices (h, k, l), and the implied sum is over the four Fe ions in sites \mathbf{d} in a magnetic unit cell. Evaluated for Fe_2TeO_6 ,

$$\Psi_Q^K(\text{TET}) = \langle O_Q^K \rangle [\gamma + \sigma_\pi \sigma_\theta \gamma^*] [1 + (-1)^n (-1)^{h+k+l}], \quad (2)$$

where the condition $Q = 2n$ on projections flows from the dyad axis of rotation symmetry on the c axis. Site symmetry demands $\sigma_\pi \sigma_\theta (-1)^{K+n} \langle O_{-Q}^K \rangle = \langle O_Q^K \rangle$. Here, σ_π and σ_θ are signatures of discrete symmetries of parity and time, with $\sigma_\pi = +1 (-1)$ for axial (polar) and $\sigma_\theta = +1 (-1)$ for time even (time odd, magnetic). The spatial phase $\gamma = \exp(i2\pi z l)$ with $z \approx 0.334$ [23].

Magnetic reflection conditions reported by Kunmann *et al.* [23] are even $h + k + l$, and odd $h + k + l$ absent. They apply to axial magnetic dipoles. The conditions are reproduced by our structure factor, Eq. (2), after setting $\sigma_\pi \sigma_\theta = -1$ and $K = 1$, and aligning dipoles with the c axis. Notably, reflections indexed $(h, k, 0)$ with $\gamma = 1$ are forbidden for all axial multipoles for all h, k .

Dirac multipoles $\langle G_Q^K \rangle$ possess $\sigma_\pi = -1$ (parity odd) and $\sigma_\theta = -1$ (magnetic) and they alone are responsible for mag-

netic Bragg reflections $(h, k, 0)$. In particular, bulk magnetic properties specified by $(0, 0, 0)$ comprise Dirac multipoles with projections even n , including magnetic monopoles. The latter are revealed by the diffraction of light using the electric dipole–magnetic dipole (E1-M1) parity-odd absorption event [8].

Here, we consider Bragg diffraction of hard x rays enhanced by the Fe K edge (energy ≈ 7.115 keV and wavelength $\lambda \approx 1.743$ Å) using an E1-E2 event [51]. Primary (secondary) photon polarizations parallel and perpendicular to the plane of scattering are labeled $\pi(\pi')$ and $\sigma(\sigma')$, respectively. The four scattering amplitudes for space group forbidden $(h, 0, 0)$ with odd h are (apart from numerical factors and radial integrals [38,52])

$$\begin{aligned} (\sigma'\sigma) &= \cos(\theta) \sin(\psi) \langle G_{+2}^2 \rangle'', \\ (\pi'\pi) &= -\cos(3\theta) \sin(\psi) \langle G_{+2}^2 \rangle'', \\ (\pi'\sigma) &= -(\sigma'\pi) = \sin(2\theta) \cos(\psi) \langle G_{+2}^2 \rangle'', \quad (h, 0, 0) \text{ odd } h. \end{aligned} \quad (3)$$

Rotation of the Fe_2TeO_6 crystal around the reflection vector is measured by the angle ψ , starting from the c axis normal to the scattering plane. The Bragg angle θ is determined by $\sin(\theta) = \lambda h / (2a) \approx h 0.189$, and $h = 1, 3, 5$ satisfy the Laue condition. To reiterate, Bragg spots $(h, 0, 0)$ with odd h are magnetic and solely determined by a Dirac quadrupole $\langle G_{+2}^2 \rangle'' = \text{Im} \langle G_{+2}^2 \rangle$. No additional information is available from Bragg spots indexed by the remaining classes of space group forbidden reflections. Equivalent reflections and absence conditions for space group $P4_2/mmm$ are listed in the Appendix for the convenience of the reader.

B. Neutron diffraction

Unlike multipoles for resonant x-ray diffraction, multipoles in neutron diffraction are strong functions of the magnitude of the reflection vector κ . Radial integrals $\langle j_c(\kappa) \rangle$ in our axial multipoles $\langle t_Q^K \rangle$ are averages of spherical Bessel functions and integer c is even. Values of $\langle j_0(\kappa) \rangle$ and $\langle j_2(\kappa) \rangle$ for ferric ions are displayed in Fig. 2 of Ref. [53]. By definition, $\langle j_c(0) \rangle = 0$ for $c > 0$, and $\langle j_0(0) \rangle = 1$. Most simple models of magnetic neutron scattering are based on the dipole $\langle t^1 \rangle$ and exclude all but $\langle j_0(\kappa) \rangle$; cf. Eq. (11) [53,54].

Magnetic and nuclear scattering amplitudes for Fe_2TeO_6 are 90° out of phase. This finding is expected on the grounds that magnetic symmetry allows the ME effect. Specifically, the identity $\{-(-1)^{K+n} \langle O_Q^K \rangle^*\} = \langle O_Q^K \rangle$ is imposed on axial multipoles by site symmetry, and the multipoles are purely real (imaginary) for odd (even) $K + n$. The Fe axial dipole ($K = 1, Q = 0$) and quadrupole ($K = 2, Q = \pm 2$) are purely real. An equivalent operator $[(\mathbf{S} \times \mathbf{R}) \mathbf{R}]$ for the quadrupole shows that it measures the correlation between a spin anapole $(\mathbf{S} \times \mathbf{R})$ and orbital degrees of freedom [55]. With $n = 1$ in Eq. (2) the quadrupole may contribute to scattering for odd $h + k + l$ and likewise for the off-diagonal octupole ($K = 3, Q = \pm 2$) that is purely imaginary.

Reflections $(0, k, l)$ odd $k + l$ are absent in nuclear scattering. The corresponding time average of the neutron scattering operator $\langle \mathbf{Q} \rangle^{(+)} = (\langle Q_x \rangle^{(+)}, 0, 0)$ [34,35,55] is purely imagi-

nary and

$$\begin{aligned} \langle Q_x \rangle^{(+)} &\approx ie_y e_z \sin(2\pi z l) [\langle t_{+2}^2 \rangle' + (1/2)\sqrt{(35/2)} \langle t_{+2}^3 \rangle''], \\ &(0, k, l) \text{ odd } k + l \end{aligned} \quad (4)$$

is correct at the level of octupoles. A unit vector \mathbf{e} is parallel to the reflection vector and components $e_y \propto k, e_z \propto l$. Since $(2\pi z) \approx 120^\circ$ the amplitude, Eq. (4), is small for Miller indices l that are multiples of 3. The superscript $(+)$ on the neutron amplitude denotes parity even. The quadrupole $\langle t_{+2}^2 \rangle'$ in Eq. (4) is proportional to the radial integral $\langle j_2(\kappa) \rangle$ that also features in the octupole $\langle t_{+2}^3 \rangle''$. It has a broad maximum around $\kappa \approx 6 \text{ \AA}^{-1}$ [53].

In general, a polarized neutron diffraction signal $\Delta = \{\mathbf{P} \cdot \langle \mathbf{Q}_\perp \rangle\}$, where \mathbf{P} is the polarization of the primary neutrons and $\langle \mathbf{Q}_\perp \rangle = \{\mathbf{e} \times (\langle \mathbf{Q} \rangle \times \mathbf{e})\}$. A spin-flip intensity SF is a measure of the magnetic content of a Bragg spot, and $\text{SF} = \{|\langle \mathbf{Q}_\perp \rangle|^2 - \Delta^2\}$ when $\mathbf{P} \cdot \mathbf{P} = 1$ and $(\langle \mathbf{Q}_\perp \rangle^* \times \langle \mathbf{Q}_\perp \rangle) = 0$ [41].

Magnetic monopoles are forbidden in $\langle \mathbf{Q}_\perp \rangle^{(-)}$ [55], and the Fe anapole ($K = 1$) is zero in Fe_2TeO_6 . In consequence, the leading contribution to diffraction by Dirac multipoles is made by the imaginary part of the spin quadrupole, $\langle g_{+2}^2 \rangle''$. The associated radial integral is zero in the forward direction of scattering [53]. Consider reflections $(0, k, l)$ absent in nuclear scattering for odd $k + l$. The component of $\langle \mathbf{Q}_\perp \rangle^{(-)}$ parallel to the a axis is different from zero, $\langle \mathbf{Q}_\perp \rangle^{(-)} = (\langle Q_{\perp,x} \rangle^{(-)}, 0, 0)$, and, neglecting Dirac multipoles beyond the mentioned quadrupole,

$$\langle Q_{\perp,x} \rangle^{(-)} \approx ie_y \cos(2\pi z l) \langle g_{+2}^2 \rangle''. \quad (5)$$

Thus

$$\text{SF} \approx |\langle Q_{\perp,x} \rangle^{(-)}|^2 (1 - P_x^2), \quad (0, k, l) \text{ odd } k + l, \quad (6)$$

and the spin-flip signal is zero for \mathbf{P} normal to the reflection vector, and potentially nonzero otherwise. Optimum intensities occur for $l = 0, 3, 6$, etc.

III. SPIN LADDER $\text{SrFe}_2\text{S}_2\text{O}$

A reduced symmetry of the orthorhombic spin ladder compound compared to tetragonal iron tellurate means fewer constraints on multipoles and diffraction amplitudes, which contain comparatively more multipoles. Diffraction by axial magnetic dipoles superimposes with core Bragg spots, as with iron tellurate, and the magnetic propagation vector = $(0, 0, 0)$ for both antiferromagnets under investigation. Equivalent reflections and absence conditions for the parent structure $Pmmn$ (No. 59) are listed in the Appendix. Cell lengths $a \approx 3.870$ Å, $b \approx 9.379$ Å, and $c \approx 6.307$ Å [28].

The magnetic space group $Pm'm'n'$ (No. 59.411, origin choice 2, BNS) of $\text{SrFe}_2\text{S}_2\text{O}$ has only recently been determined [28]. It is centrosymmetric and belongs to the magnetic crystal class $m'm'm'$ that forbids a piezomagnetic effect. The antiferromagnetic configuration of axial dipoles normal to the a axis below $T_N \approx 216$ K is depicted in Fig. 2. The refined magnetic structure implies the magnetic axial dipole along the b axis to be the primary order parameter, which defines the $Pm'm'n'$ space group. The latter allows the orthogonal axial component along the c axis as a secondary order parameter

coupled to the primary one via a weak interaction, e.g., the Dzyaloshinskii-Moriya interaction. Unlike tetragonal iron tellurate, there are three independent parameters in the diagonal ME coupling tensor, and the magnetic crystal class $m' m' m'$ is one of three with no bulk axial magnetism that allow the Kerr effect [56]. Anapoles (Dirac dipoles) are another feature of the spin ladder compound not present in iron tellurate.

Ferrous ions Fe^{2+} ($3d^6$) use Wyckoff sites $4(e)$ with symmetry m'_x (mirror and time-reversal invariances along the a axis in Fig. 2). An electronic structure factor for a reflection vector (h, k, l) with integer Miller indices is as follows:

$$\Psi_Q^K(\text{ORH}) = \exp(i\pi h/2) \langle O_Q^K \rangle [\beta + \beta^*(-1)^{Q+k}] \times [\gamma + \sigma_\pi \sigma_\theta \gamma^*(-1)^Q (-1)^{h+k}]. \quad (7)$$

Site symmetry for ferrous ions demands $\sigma_\pi \sigma_\theta (-1)^K \langle O_{-Q}^K \rangle = \langle O_Q^K \rangle$, while $(-1)^Q \langle O_{-Q}^K \rangle^* = \langle O_Q^K \rangle$ and $\sigma_\pi \sigma_\theta = -1$ ($+1$) for axial (Dirac) multipoles, respectively. Spatial phases in Eq. (7) are $\beta = \exp(i2\pi yk)$, $\gamma = \exp(i2\pi zl)$ with $y \approx 0.582$ and $z \approx 0.378$ [28].

Axial multipoles with even (odd) $K + Q$ are purely imaginary (real). The classification is reversed for Dirac multipoles. Cartesian components (x, y, z) of a dipole are derived from $\langle O_x^1 \rangle = (\langle O_{-1}^1 \rangle - \langle O_{+1}^1 \rangle) / \sqrt{2} = -\sqrt{2} \langle O_{+1}^1 \rangle'$, $\langle O_y^1 \rangle = i(\langle O_{-1}^1 \rangle + \langle O_{+1}^1 \rangle) / \sqrt{2} = -\sqrt{2} \langle O_{+1}^1 \rangle''$, and $\langle O_z^1 \rangle = \langle O_0^1 \rangle$. Anapoles are normal to the b - c plane that contains axial dipoles. Bulk magnetic properties comprise Dirac multipoles with projections even Q , and include the monopole (\mathbf{G}^0) and quadrupoles (\mathbf{G}^2).

A. X-ray diffraction

Diffraction enhanced by a parity-even absorption event is allowed at space group forbidden reflections, in contrast to iron tellurate. The Fe L_2 edge has an energy 721 eV, $\lambda/(2b) \approx 0.917$, and $k = 1$ is allowed in $(0, k, 0)$. The E1-E1 amplitude in the rotated channel of polarization ($\pi'\sigma$) is proportional to the axial moment parallel to the c axis, and the corresponding multipole is denoted $\langle T_z^1 \rangle$ in amplitudes,

$$(\pi'\sigma) = -(\sigma'\pi) = \sin(2\pi y) \cos(\theta) \sin(\psi) \langle T_z^1 \rangle, \quad (0, 1, 0), \quad (8)$$

with $\sin(2\pi y) = -0.493$. Axial octupoles are engaged in diffraction by an E2-E2 event at the Fe K edge [38,57,58] with the result

$$\begin{aligned} (\pi'\sigma) = -(\sigma'\pi) = & -\sin(2\pi yk) \sin(\psi) [\cos(3\theta) \langle T_z^1 \rangle \\ & + \{3 \cos(3\theta) + 5\Phi \sin^2(\psi)\} \langle T_0^3 \rangle \\ & - \sqrt{30} \{\cos(\theta) \cos(2\theta) + \Phi \sin^2(\psi)\} \langle T_{+2}^3 \rangle'], \end{aligned} \quad (9)$$

(0, k , 0) odd k ,

where $\Phi = \{\cos(\theta) [2 - 3 \cos^2(\theta)]\}$. E2-E2 amplitudes, Eq. (9), are potentially strong for $(0, 3, 0)$, for which $\sin(6\pi y) \approx -1.0$, $\cos(3\theta) \approx 0.662$, $\cos(\theta) \cos(2\theta) \approx 0.811$, and $\Phi \approx -0.737$. Moreover, diffraction by Dirac multipoles using the event E1-E2 is negligible for $(0, 3, 0)$, as we shall see. The condition $\sin(\theta) = \lambda k / (2b) \approx k 0.093$ is satisfied for $k = 1, 3, 5, 7, 9$. Contributions $\langle T_z^1 \rangle$ in Eqs. (8) and (9) merit

comment, which is found following Eq. (11) in the following subsection.

In discussing diffraction by Dirac multipoles, we continue to explore space group forbidden reflections. The structure factor, Eq. (7), is zero for $(h, 0, 0)$ with odd h . Projections Q are restricted to odd values for $(0, k, 0)$ with odd k , and in the rotated E1-E2 channel,

$$\begin{aligned} (\pi'\sigma) = -(\sigma'\pi) = & \cos(2\pi yk) \sin(2\theta) \sin(\psi) \\ & \times [3 \langle G_{+1}^1 \rangle' + 2\sqrt{5} \langle G_{+1}^2 \rangle'' + \{4 - 15 \cos^2(\psi)\} \langle G_{+1}^3 \rangle' \\ & + \sqrt{15} \cos^2(\psi) \langle G_{+3}^3 \rangle'], \quad (0, k, 0) \text{ odd } k. \end{aligned} \quad (10)$$

As previously mentioned, $\cos(6\pi y) \approx 0.0$. Miller index $k = 7$ is optimum for the prefactors $\sin(2\theta)$ and $\cos(2\pi yk)$. Note that a quadrupole is absent from the E2-E2 amplitude, Eq. (9), because magnetic parity-even diffraction uses odd rank multipoles alone.

B. Neutron diffraction

For $(0, k, 0)$ with odd k , $\langle \mathbf{Q} \rangle^{(+)} = (0, 0, \langle Q_z \rangle^{(+)})$ is purely imaginary, as expected, and

$$\begin{aligned} \langle Q_z \rangle^{(+)} \approx & i \sin(2\pi yk) [\langle t_z^1 \rangle - (2/\sqrt{3}) \langle t_{+2}^2 \rangle'' \\ & - (1/4) \sqrt{7} \langle t_0^3 \rangle + 2\sqrt{5/6} \langle t_{+2}^3 \rangle'] \quad (0, k, 0) \text{ odd } k. \end{aligned} \quad (11)$$

The result is correct for all multipoles up to and including $K = 3$. The presence in Eq. (11) of the axial magnetic dipole appears, at first sight, to be at odds with the conclusion by Guo *et al.* [28] that chemical and magnetic dipole structures match. Two elementary resolutions are (i) the component of the axial dipole $\langle t_z^1 \rangle$ parallel to the c axis is zero, or (ii) $\langle t_z^1 \rangle$ is too small to be detected with the resolution available to Guo *et al.* [28]. As it stands, dipoles $\langle t_y^1 \rangle$ constitute the primary order parameter, with $\langle t_z^1 \rangle$ contributing a comparatively weak secondary order parameter. Note, while Fe site symmetry m'_x allows $\langle t_z^1 \rangle$ it can be identically zero. Returning to Fe_2TeO_6 , the predicted magnetic amplitude Eq. (4) for noncore Bragg spots has the expected structure, i.e., no axial dipoles. Intensity of a Bragg spot = $|\langle Q_z \rangle^{(+)}|^2$ since $\langle \mathbf{Q} \rangle^{(+)}$ and \mathbf{e} are orthogonal.

The result in Eq. (11) holds for $(h, 0, 0)$ with $h = (2n + 1)$ on making one change. The spatial phase factor $\sin(2\pi yk)$ is replaced by $(-1)^n$.

An approximation for the axial dipole in Eq. (11),

$$\langle t_z^1 \rangle \approx (\langle \boldsymbol{\mu} \rangle / 3) [\langle j_0(\kappa) \rangle + \langle j_2(\kappa) \rangle (g - 2) / g], \quad (12)$$

is often used [34,55]. Here, the magnetic moment $\langle \boldsymbol{\mu} \rangle = g \langle \mathbf{S} \rangle$ and the orbital moment $\langle \mathbf{L} \rangle = (g - 2) \langle \mathbf{S} \rangle$.

Regarding diffraction by Dirac multipoles, $\langle \mathbf{Q}_{\perp,z} \rangle^{(-)} = (0, 0, \langle Q_{\perp,z} \rangle^{(-)})$ for $(0, k, 0)$ with odd k . At an accuracy that includes anapoles and quadrupoles,

$$\langle Q_{\perp,z} \rangle^{(-)} \approx -i \cos(2\pi yk) \langle g_{+1}^2 \rangle'', \quad (0, k, 0) \text{ odd } k. \quad (13)$$

The spatial phase factor is zero for $k = 3$, to a good approximation, while Eq. (11) for the axial contribution to diffraction is optimal.

IV. DISCUSSION

In summary, we have identified Dirac multipoles in two antiferromagnetic iron-based magnetoelectric (ME) compounds cited in Table I, and depicted in Figs. 1 and 2. They are polar and magnetic (time odd), and represent the scalar, dipole, and quadrupole in a decomposition of the third-order tensor that couples electric and magnetic fields in Landau free energy. Findings are informed by symmetry in previously established magnetic space groups for iron tellurate [23] and a spin ladder compound [28]. A linear ME effect in iron tellurate has been thoroughly investigated, starting in 1972 with a study reported by Buksphan *et al.* [24]. This is not so for the spin ladder $\text{SrFe}_2\text{S}_2\text{O}$, to the best of our knowledge. However, its magnetic space group belongs to the crystal class $m'm'm'$ that allows a linear ME effect. Even more interestingly, the magnetic crystal class is one of three with no bulk axial magnetism that allow the Kerr effect [56]. Dirac multipoles form bulk magnetization in both iron-based compounds, and it includes monopoles (often called magnetic charges).

The published magnetic space group $Pm'm'n'$ for the ladder compound implies that magnetic axial dipoles along the b axis in Fig. 2 form a primary order parameter. This space group also allows an orthogonal axial component along the c axis. The latter seems to be a secondary order parameter weakly coupled to the primary one and therefore too small to be reliably detected in a neutron diffraction experiment on a powder sample [28]. Usually, orthogonal magnetic components due to spin canting imposed by the Dzyaloshinskii-Moriya interaction are roughly about $0.01\text{--}0.02\ \mu\text{B}$, which is almost an order of magnitude smaller than the sensitivity of good quality powder diffraction data [59].

The defining property of magnetoelectric space groups is the presence of anti-inversion ($\bar{1}'$) among invariance requirements. It has global influence on diffraction amplitudes for antiferromagnetic materials, which is illustrated by our results. Nuclear and magnetic contributions to the neutron scattering amplitude are forced to differ by 90° . In the diffraction of x rays with energy matching an iron resonance charge and magnetic contributions have a like phase. In consequence,

Bragg diffraction patterns are independent of helicity carried by primary x rays.

Special attention in our calculations is given to weak Bragg spots stemming from angular anisotropy in magnetic distributions. Such reflections violate absence conditions derived from diffraction patterns generated by nuclei or spherical distributions of electronic charge, which are listed in the Appendix together with reflection equivalences. Weak Bragg spots reveal fine details of the distribution of magnetization in a crystal. They feature axial quadrupoles, the correlation between a spin anapole and orbital degrees of freedom, anapoles, and Dirac quadrupoles. Calculated x-ray diffraction patterns include the effect of rotating the crystal about the reflection vector (an azimuthal-angle scan) that reveals magnetic symmetries.

ACKNOWLEDGMENTS

Dr. K. S. Knight and Dr. D. D. Khalyavin were generous with guidance on crystal and magnetic symmetries in calculations of Bragg diffraction patterns. Professor S. P. Collins commented on the feasibility of proposed x-ray Bragg diffraction experiments.

APPENDIX

Equivalent reflections for $P4_2/mmm$ (No. 136):

- (1) h, k, l ; (2) $-h, -k, l$; (3) $-k, h, l$; (4) $k, -h, l$;
 (5) $-h, k, -l$; (6) $h, -k, -l$; (7) $k, h, -l$; (8) $-k, -h, -l$;
 (9) $-h, -k, -l$; (10) $h, k, -l$; (11) $k, -h, -l$;
 (12) $-k, h, -l$;
 (13) $h, -k, l$; (14) $-h, k, l$; (15) $-k, -h, l$; (16) k, h, l ;
 (0, 0, l) odd l absent; (h , 0, 0) odd h absent; (0, k , l) odd $k + l$ absent.

Equivalent reflections for $Pm\bar{m}n$ (No. 59):

- (1) h, k, l ; (2) $-h, -k, l$; (3) $-h, k, -l$; (4) $h, -k, -l$;
 (5) $-h, -k, -l$; (6) $h, k, -l$; (7) $h, -k, l$; (8) $-h, k, l$;
 ($h, k, 0$) odd $h + k$ absent; ($h, 0, 0$) odd h absent; (0, $k, 0$) odd k absent.

- [1] I. E. Dzyaloshinskii, Zh. Eksp. Teor. Fiz. **37**, 881 (1959) [Sov. Phys. JETP **10**, 628 (1960)].
 [2] D. N. Astrov, Zh. Eksp. Teor. Fiz. **38**, 984 (1960) [Sov. Phys. JETP **11**, 708 (1960)].
 [3] H. Schmid, *Ferroelectrics* **161**, 1 (1994).
 [4] M. Bichurin, *Ferroelectrics* **204**, xvii (1997).
 [5] P. J. Brown, J. B. Forsyth, E. Lelièvre-Berna, and F. Tasset, *J. Phys.: Condens. Matter* **14**, 1957 (2002).
 [6] J. A. Blanco, P. J. Brown, A. Stunault, K. Katsumata, F. Iga, and S. Michimura, *Phys. Rev. B* **73**, 212411 (2006).
 [7] A. S. Goldhaber, *Phys. Rev. D* **16**, 1815 (1977).
 [8] J. I. Igarashi and T. Nagao, *Phys. Rev. B* **80**, 054418 (2009).
 [9] S. W. Lovesey and V. Scagnoli, *J. Phys.: Condens. Matter* **21**, 474214 (2009).
 [10] S. W. Lovesey and D. D. Khalyavin, *J. Phys. Soc. Jpn.* **82**, 103703 (2013).
 [11] K. A. Milton, *Rep. Prog. Phys.* **69**, 1637 (2006).
 [12] Y. B. Zel'dovich, Zh. Eksp. Teor. Fiz. **33**, 1531 (1957) [Sov. Phys. JETP **6**, 1184 (1958)].
 [13] S. W. Lovesey, E. Balcar, K. S. Knight, and J. F. Rodriguez, *Phys. Rep.* **411**, 233 (2005).
 [14] N. A. Spaldin, M. Fiebig, and M. Mostovoy, *J. Phys.: Condens. Matter* **20**, 434203 (2008).
 [15] J. Fernández-Rodríguez, V. Scagnoli, C. Mazzoli, F. Fabrizi, S. W. Lovesey, J. A. Blanco, D. S. Sivia, K. S. Knight, F. de Bergevin, and L. Paolasini, *Phys. Rev. B* **81**, 085107 (2010).
 [16] V. Scagnoli, U. Staub, Y. Bodenthin, R. A. de Souza, M. García-Fernández, M. Garganourakis, A. T. Boothroyd, D. Prabhakaran, and S. W. Lovesey, *Science* **332**, 696 (2011).
 [17] S. W. Lovesey, T. Chatterji, A. Stunault, D. D. Khalyavin, and G. van der Laan, *Phys. Rev. Lett.* **122**, 047203 (2019).
 [18] S. P. Collins, D. Laundy, T. Connolley, G. van der Laan, F. Fabrizi, O. Janssen, M. J. Cooper, H. Ebert, and S.

- Mankovsky, *Acta Crystallogr., Sect. A: Found. Adv.* **72**, 197 (2016).
- [19] S. Bhowal, S. P. Collins, and N. A. Spaldin, *Phys. Rev. Lett.* **128**, 116402 (2022).
- [20] O. Bunau and Y. Joly, *J. Phys.: Condens. Matter* **21**, 345501 (2009).
- [21] N. A. Spaldin, M. Fechner, E. Bousquet, A. Balatsky, and L. Nordström, *Phys. Rev. B* **88**, 094429 (2013).
- [22] M. Ramakrishnan, Y. Joly, Q. N. Meier, M. Fechner, M. Porer, S. Parchenko, Y. W. Windsor, E. M. Bothschafter, F. Lichtenberg, and U. Staub, *Phys. Rev. Res.* **5**, 013203 (2023).
- [23] W. Kunmann, S. La Placa, L. M. Corliss, J. M. Hastings, and E. Banks, *J. Phys. Chem. Solids* **29**, 1359 (1968).
- [24] S. Buksphan, E. Fischer, and R. M. Hornreich, *Solid State Comm.* **10**, 657 (1972).
- [25] S. Mu and K. D. Belashchenko, *J. Phys.: Condens. Matter* **27**, 022203 (2015).
- [26] J. Wang, J. A. C. Santana, N. Wu, C. Karunakaran, J. Wang, P. A. Dowben, and C. J. Binck, *J. Phys.: Condens. Matter* **26**, 055012 (2014).
- [27] S. D. Kaushik, B. Sahu, S. R. Mohapatra, and A. K. Singh, in *DAE Solid State Physics Symposium*, edited by R. Chitra, S. Bhattacharya, and N. K. Sahoo, AIP Conf. Proc. No. 1731 (AIP, Melville, NY, 2015), p. 130037.
- [28] H. Guo *et al.*, *Eur. J. Inorg. Chem.* **32**, 3829 (2017).
- [29] MAGNDATA, <http://webbdcristal.ehu.es/magndata>.
- [30] S. W. Lovesey, D. D. Khalyavin, and G. van der Laan, *Phys. Rev. B* **105**, 014403 (2022).
- [31] H. A. Alperin, P. J. Brown, R. Nathans, and S. J. Pickart, *Phys. Rev. Lett.* **8**, 237 (1962).
- [32] P. J. Brown, *Phys. B (Amsterdam)* **192**, 14 (1993).
- [33] R. M. Moon, T. Riste, and W. C. Koehler, *Phys. Rev.* **181**, 920 (1969).
- [34] S. W. Lovesey, *Theory of Neutron Scattering from Condensed Matter* (Clarendon Press, Oxford, 1987), Vol. 2.
- [35] A. T. Boothroyd, *Principles of Neutron Scattering from Condensed Matter* (Oxford University Press, Oxford, 2020).
- [36] D. H. Templeton and L. K. Templeton, *Acta Crystallogr., Sect. A* **41**, 133 (1985); D. H. Templeton, and L. K. Templeton, **42**, 478 (1986); with a review by V. E. Dmitrienko, K. Ishida, A. Kirfel, and N. E. Ovchinnikova, *Acta Crystallogr., Sect. A* **61**, 481 (2005).
- [37] D. H. Templeton, in *Handbook on Synchrotron Radiation*, edited by G. Brown and D. E. Moncton (Elsevier Science, New York, 1991), Vol. 3.
- [38] V. Scagnoli and S. W. Lovesey, *Phys. Rev. B* **79**, 035111 (2009).
- [39] T. P. Croft, E. Blackburn, J. Kulda, R. Liang, D. A. Bonn, W. N. Hardy, and S. M. Hayden, *Phys. Rev. B* **96**, 214504 (2017).
- [40] P. Bourges, Y. Sidis, and L. Mangin-Thro, *Phys. Rev. B* **98**, 016501 (2018).
- [41] P. Bourges, D. Bounoua, and Y. Sidis, *C. R. Phys.* **22**, 1 (2021).
- [42] S. W. Lovesey, D. D. Khalyavin, and U. Staub, *J. Phys.: Condens. Matter* **27**, 292201 (2015).
- [43] S. W. Lovesey and D. D. Khalyavin, *J. Phys.: Condens. Matter* **27**, 495601 (2015).
- [44] E. C. Schueller, Y. M. Oey, K. D. Miller, K. E. Wyckoff, R. Zhang, W. Zhan, S. D. Wilson, J. M. Rondinell, and R. Seshadri, *Inorg. Chem.* **60**, 9224 (2021).
- [45] E. A. Turov and V. V. Nikolaev, *Phys.-Usp.* **48**, 431 (2005).
- [46] N. Matsubara, F. Damay, B. Vertruyen, N. Barrier, O. I. Lebedev, P. Boullay, E. Elkaim, P. Manuel, D. D. Khalyavin, and C. Martin, *Inorg. Chem.* **56**, 9742 (2017).
- [47] Y. Fang, L. Y. Wang, Y. Q. Song, T. Tang, D. H. Wang, and Y. W. Du, *Appl. Phys. Lett.* **104**, 132908 (2014).
- [48] M. W. Gaultois, M. C. Kemei, J. K. Harada, and R. Seshadri, *J. Appl. Phys.* **117**, 014105 (2015).
- [49] We use the BNS setting of magnetic space groups; see Bilbao Crystallographic server, <https://www.cryst.ehu.es/>.
- [50] P. Fabrykiewicz, R. Przeniosło, I. Sosnowska, and D. Oleszak, *Acta Crystallogr., Sect. A* **75**, 889 (2019).
- [51] A. Rodríguez-Fernández, J. A. Blanco, S. W. Lovesey, V. Scagnoli, U. Staub, H. C. Walker, D. K. Shukla, and J. Stremper, *Phys. Rev. B* **88**, 094437 (2013).
- [52] S. W. Lovesey and G. van der Laan, *Phys. Rev. B* **100**, 245112 (2019).
- [53] S. W. Lovesey, *Phys. Rev. B* **106**, 064415 (2022).
- [54] O. Halpern and M. H. Johnson, *Phys. Rev.* **55**, 818 (1938).
- [55] S. W. Lovesey, *Phys. Scr.* **90**, 108011 (2015).
- [56] J. Orenstein, *Phys. Rev. Lett.* **107**, 067002 (2011).
- [57] K. D. Finkelstein, Q. Shen, and S. Shastri, *Phys. Rev. Lett.* **69**, 1612 (1992).
- [58] J. P. Hill, C.-C. Kao, and D. F. McMorrow, *Phys. Rev. B* **55**, R8662(R) (1997).
- [59] Dr. D. D. Khalyavin (private communication).